

Proceedings of the Institution of Mechanical Engineers, Part K: Journal of Multi-body Dynamics

<http://pik.sagepub.com/>

Rider control identification in bicycling using lateral force perturbation tests

AL Schwab, PDL de Lange, R Happee and Jason K Moore

Proceedings of the Institution of Mechanical Engineers, Part K: Journal of Multi-body Dynamics published online 27 August 2013

DOI: 10.1177/1464419313492317

The online version of this article can be found at:

<http://pik.sagepub.com/content/early/2013/08/26/1464419313492317>

Published by:



<http://www.sagepublications.com>

On behalf of:



[Institution of Mechanical Engineers](http://www.institutionofmechanicalengineers.org)

Additional services and information for *Proceedings of the Institution of Mechanical Engineers, Part K: Journal of Multi-body Dynamics* can be found at:

Email Alerts: <http://pik.sagepub.com/cgi/alerts>

Subscriptions: <http://pik.sagepub.com/subscriptions>

Reprints: <http://www.sagepub.com/journalsReprints.nav>

Permissions: <http://www.sagepub.com/journalsPermissions.nav>

>> [OnlineFirst Version of Record](#) - Aug 27, 2013

[What is This?](#)

Rider control identification in bicycling using lateral force perturbation tests

AL Schwab¹, PDL de Lange¹, R Happee¹ and Jason K Moore²

Proc IMechE Part K:
J Multi-body Dynamics
0(0) 1–17
© IMechE 2013
Reprints and permissions:
sagepub.co.uk/journalsPermissions.nav
DOI: 10.1177/1464419313492317
pik.sagepub.com



Abstract

A model describing rider control while steering and stabilizing a bicycle has been developed. Experimental data were obtained from riding a bicycle on a narrow treadmill while perturbing balance with impulsive forces at the seat post. The experiments were conducted at 2–7 m/s covering both the stable and the unstable forward speed range. Bicycle and rider mechanics have been modeled using the Whipple bicycle model extended with the rider inertia. A rider control model applying steering torque at the handle bars has been developed exploring potential feedback of visual, vestibular and arm proprioceptive cues. The identified rider control parameters, after model reduction, stabilize the system and mimic realistic rider control behavior. The feedback gains of this control model were used to identify the specific optimal control linear-quadratic regulator (LQR) cost function which the rider was using to control the bicycle. The identified cost functions indicate that at low speed the rider minimizes his control effort and at high speed he minimizes the heading error.

Keywords

Bicycle, dynamics, manual control, system identification, rider model, optimal control

Date received: 6 February 2013; accepted: 8 May 2013

Introduction

Balancing a bicycle in motion is an acquired skill which is poorly understood. Multibody dynamic models of uncontrolled bicycles have provided fundamental insight into bicycle stability in relation to speed and geometry.^{1,2} Further insight into human control is needed to design bicycles that minimize the risk of falling, possibly utilizing automatic or assisting control. In particular, we need to better understand which sensory information is used by the rider, and how this information is used in the combined steering and stabilization task.

Research in manual control of bicycles and motorcycles started in the 1970s during the renewed interest in cybernetics.^{3–6} Among the first were Van Lunteren and Stassen³ who used a stationary bicycle simulator, mimicking normal bicycling, to investigate the influence of drugs and alcohol on the performance of the rider. With the same simulator they used system identification techniques to identify the rider control at one fixed forward speed, where they adequately described the rider as a linear proportional–integral–derivative (PID) controller with delay. Rice and Roland⁴ measured rider control behavior after an initial lateral perturbation at various speeds on various bicycles and compared the results to computer simulations. Weir⁵ used a computer model of a motorcycle rider combination to identify the transfer functions of the various control input–output

relations, and concluded that steer torque response to lean angle error is the easiest way to balance a motorcycle in motion. The first to actually validate a rider–vehicle model was Eaton,⁶ who carried out experiments to validate the theoretical Sharp⁷ motorcycle model (including tires) and the rider control crossover model by Weir.⁵ After these pioneering studies, most attention has been directed to high-speed motorcycle rider control for reasons of traffic safety.⁸ However, the act of balancing at low speed, as is the case for bicycles, has been given little attention. Only in this decade, the research on low-speed human rider control in bicycling was started again at TU Delft and UC Davis, by observing motions of various rider–bicycle combinations while balancing a bicycle in motion on a large treadmill⁹ and the application of modern manual control models.¹⁰

Currently there are two main modeling approaches on human rider control in bicycling. One builds on the

¹Laboratory for Engineering Mechanics & BioMechanical Engineering, Delft University of Technology, Mekelweg, CD Delft, The Netherlands

²Sports Biomechanics Lab, Mechanical and Aerospace Engineering, University of California, Davis, CA, USA

Corresponding author:

AL Schwab, Laboratory for Engineering Mechanics & BioMechanical Engineering, Delft University of Technology, Mekelweg 2, NL 2628 CD Delft, The Netherlands.

Email: a.l.schwab@tudelft.nl

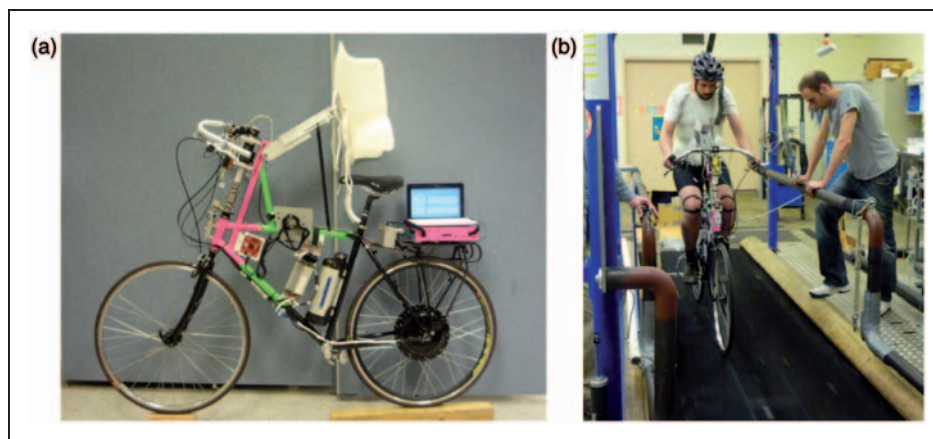


Figure 1. (a) Instrumented and actuated measurement bicycle with rigid rider harness, parameters according to Table 6 and system matrices according to Table 7 and (b) experimental setup at UC Davis of an instrumented and actuated bicycle riding on a narrow treadmill. The lateral perturbation is an impulsive pulling/pushing force at the seat post. The instrumentation of this bicycle is described in detail in ref. ¹⁸

well-developed quasi-linear aircraft pilot and car driver model as developed by McRuer et al.^{11–13} and are transferred to the control of a bicycle. The other is more about intermittent control, where the rider has no action until a certain threshold and then performs an impulsive like action.¹⁴ Such systems are essentially nonlinear, and parallels can be drawn with recent human postural balance research by Milton.¹⁵ In the work presented here, which elaborates on ref.,¹⁶ we have investigated the validity of the first type of models, that is, a linear controller exploring potential feedback of visual, vestibular and arm proprioceptive cues.

The outline of this article is as follows. After this introduction the model of the bicycle–rider combination which is used in the system identification process is presented. Then the system identification method used herein is presented. Next, the experimental measurements are briefly discussed after which the identified models are presented. Then with the help of optimal control theory the question ‘what does the rider optimize?’ is addressed. This article ends with a discussion and conclusions.

Approach

For the rider control model we assume a linear PID controller with or without delay, where the control inputs are the bicycle lean and steer angle with their higher derivatives, and the control output is the steer torque. The rider is assumed to be rigidly attached to the rear frame. Experimental data were obtained at UC Davis.^{17,18} In the experiments used here, the bicycle is ridden on a narrow, 1-m wide, treadmill and intermittently laterally perturbed by an impulsive force at the seat post; this is further explained in the next section. For the rider model system identification, first a black box finite impulse response (FIR) model is fit to the data, which served as a platform for subsequent

identification of the rider control parameters. Next, a gray box model is fit to the response of the FIR model. Finally, the identified feedback gains are used to compute the specific optimal control linear-quadratic regulator (LQR) cost function which the rider is using to control the bicycle. This is described in detail in the ‘System model’ and ‘System identification’ sections.

Experimental setup

At UC Davis, a measurement bicycle has been constructed, which is fully equipped with a number of sensors to measure the state and rider input, see Figure 1. In addition, a perturber mechanism is present, which is used to excite the system. These perturbations are applied by laterally pushing or pulling a rod with a force sensor in series, which is attached on the seat post. The measurement bicycle has the following characteristics: the upper body lean relative to the rear frame is constrained by rigidly fixing the upper body with a harness to the bicycle frame in order to mimic the rigid rider bicycle model (Whipple model) as best as possible. Next, the knees are fixed to the bicycle frame, which prevents the lateral knee movement which was observed by Moore et al.,⁹ and the bicycle is electrically driven, so the rider does not need to exert pedaling power and thus eliminates the need for lower limb movement. The rider was only able to move his arms from shoulder down and his head. The instrumentation of this bicycle is described in detail in ref. ¹⁸

Initially two different types of experiments are performed; lateral line tracking and roll stabilization of which only the latter is used here. The experiments are performed in two environments: on a horse treadmill and at a gymnasium. The horse treadmill proved to be more suitable for the perturbation experiments, since it is easier to perturb a stationary positioned bicycle by pulling/pushing a rod. A downside of this

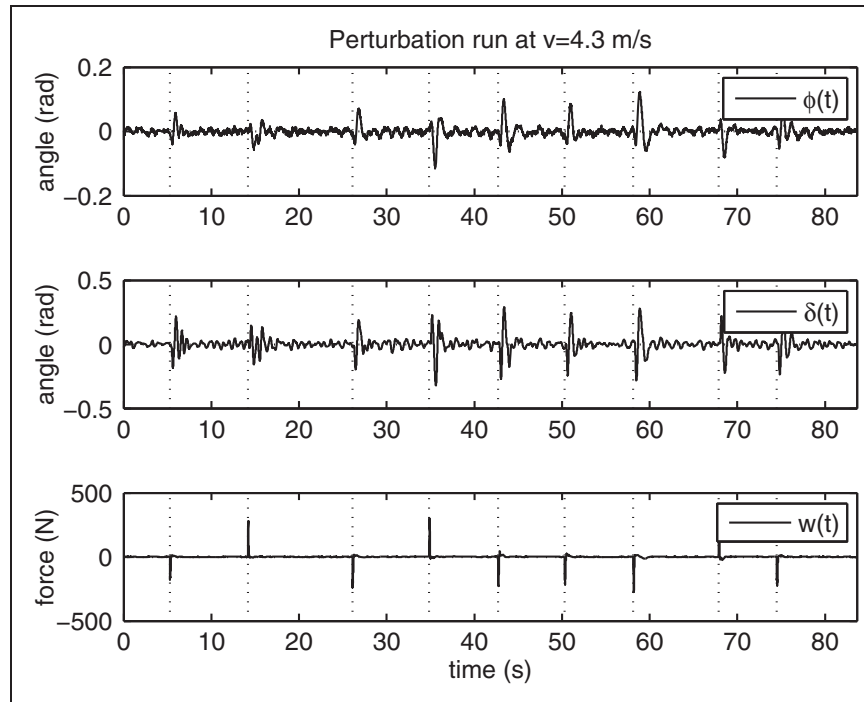


Figure 2. Measurements of the rear frame roll angle ϕ (top), steering angle δ (middle) and disturbance w (bottom) as a function of time, for a forward velocity of 4.3 m/s (run 252).

environment is the rather narrow track, resulting in a stressful and unnatural overly concentrated way of bicycling, which in particular at high speed, turned the roll stabilization more into heading tracking. The treadmill perturbation experiments are performed at forward velocities of about 2, 3, 4, 6 and 7 m/s with a measurement time of 60–90 s, each of them is repeated a number of times.

The raw measured data during the experiments were processed into these time series: the forward velocity v , the rear frame roll angle ϕ and roll rate $\dot{\phi}$, the steer angle δ and steer rate $\dot{\delta}$, the disturbance force applied at the seat post w and the steering torque T_δ , see ref. ¹⁸ for details. Unfortunately, the measured steering torque did not well match the torque needed to drive the Whipple model in the same trajectory, where the measured torque exceeded the model torque by a factor of 2–3. Hence, the measured torque was not used in the identification process. The discrepancy could be attributed to measurement errors, or limitations in the Whipple model, such as neglected tire dynamics. Figure 2 shows a typical measurement of the roll angle, steering angle and input force.

For further analysis, measured data from 15 trials are chosen, these runs are shown in Table 1. These 15 trials are chosen, because they are well spread over the forward speed range and show a clear input/output relationship, which allows for proper system identification. The corresponding data for these trials are publicly available and can be downloaded from ref. ¹⁷

The dynamic model of the bicycle rider combination is presented in the next section, where the

Table 1. Experimental runs used in this study with: run id, rider name, forward speed, duration, and date and time of the experiment. These were all done on a narrow treadmill for a balancing task.

Run id	Rider	v (m/s)	T (s)	Date and time
248	Jason	2.1	90	30-Aug-2011 11:24:37
249	Jason	2.2	90	30-Aug-2011 11:27:20
250	Jason	2.2	90	30-Aug-2011 11:30:51
184	Jason	3.2	60	09-Mar-2011 17:04:38
185	Jason	3.2	60	09-Mar-2011 17:09:20
186	Jason	3.1	60	09-Mar-2011 17:12:33
251	Jason	4.3	90	30-Aug-2011 11:33:18
252	Jason	4.3	90	30-Aug-2011 11:36:16
253	Jason	4.3	90	30-Aug-2011 11:39:57
190	Jason	6.0	60	09-Mar-2011 17:24:22
191	Jason	6.1	60	09-Mar-2011 17:26:39
192	Jason	6.1	60	09-Mar-2011 17:28:39
255	Jason	7.3	90	30-Aug-2011 12:07:37
256	Jason	7.3	90	30-Aug-2011 12:10:12
257	Jason	7.4	90	30-Aug-2011 12:17:47

dimensions and inertial properties of the bicycle are measured according to Moore et al. ^{18,19} The resulting parameters for the rigid rider (Whipple) bicycle model are presented in Table 6 of the appendix, whereas the corresponding mass, damping and stiffness matrices together with the disturbance force transfer matrix

are shown in Table 7 of the appendix. Note from the transfer function \mathbf{H}_{fv} from Table 7 of the appendix, that the lateral force w contributes mainly to the generalized lean torque T_ϕ and little to the generalized steer torque T_δ . This makes sense, because the rope is attached under the rider seat and is pulled in a lateral direction, which mainly causes a roll torque and little steering.

System model

The total system is a combination of a bicycle and rider. For the bicycle the Whipple rigid rider model will be used, whereas the rider control will be modeled as a linear feedback control system with inherent neuromuscular lag.

Bicycle model

The bicycle model used is the so-called Whipple model,²⁰ which recently has been benchmarked by Meijaard et al.¹ The model, see Figure 3, consists of four rigid bodies connected by three revolute joints. The contact between the knife-edged wheels and the flat level surface is modeled by holonomic constraints in the normal direction, prescribing the wheels to touch the surface, and by non-holonomic constraints in the longitudinal and lateral directions, prescribing zero longitudinal and lateral slips. In this original model, it is assumed that the rider is rigidly attached to the rear frame and has no hands on the handlebar. The resulting non-holonomic mechanical model has three velocity degrees of freedom: forward speed v , rear frame roll rate $\dot{\phi}$ and steering rate $\dot{\delta}$.

The lateral motions can be described by the linearized equations of motion for small perturbations about the upright steady forward motion. These linearized equations of motion are fully described by Meijaard et al.¹ They are expressed in terms of small

changes in the lateral degrees of freedom (the rear frame roll angle, ϕ , and the steering angle, δ) from the upright straight-ahead configuration $(\phi, \delta) = (0, 0)$, at a forward speed v , and have the form

$$\mathbf{M}\ddot{\mathbf{q}} + v\mathbf{C}_1\dot{\mathbf{q}} + [g\mathbf{K}_0 + v^2\mathbf{K}_2]\mathbf{q} = \mathbf{f} \quad (1)$$

where the time-varying variables are $\mathbf{q} = [\phi, \delta]^T$ and the lean and steering torques are $\mathbf{f} = [T_\phi, T_\delta]^T$. The coefficients in this equation are: a constant symmetric mass matrix, \mathbf{M} , a damping-like (there is no real damping) matrix, $v\mathbf{C}_1$, which is linear in the forward speed v , and a stiffness matrix which is the sum of a constant symmetric part, $g\mathbf{K}_0$, and a part, $v^2\mathbf{K}_2$, which is quadratic in the forward speed. The forces on the right-hand side, \mathbf{f} , are the applied forces which are energetically dual to the degrees of freedom \mathbf{q} . In the upright straight-ahead configuration, the linearized equation of motion for the forward motion is decoupled from the linearized equations of motion of the lateral motions and simply reads $\dot{v} = 0$.

Besides the equations of motion, kinematic differential equations for the configuration variables that are not degrees of freedom have to be added to complete the description. For the forward motion, the equations for the rotational angular rates of the wheels are $\dot{\theta}_R = -v/r_R$, $\dot{\theta}_F = -v/r_F$, where θ_R and θ_F are the rotation angles of the rear and front wheel and r_R and r_F are the corresponding wheel radii. For the lateral motion, the equations for the yaw (heading) angle, ψ , and the lateral displacement of the rear and front wheel contact point, y_P and y_Q , are

$$\dot{\psi} = (v\delta + c\dot{\delta}) \cos \lambda_s / w \quad (2)$$

$$\dot{y}_P = v\psi \quad (3)$$

$$\dot{y}_Q = y_P + w\psi - c\dot{\delta} \cos \lambda_s \quad (4)$$

with wheelbase w , trail c and steer axis tilt λ_s . For the case of the bicycle, these equations can be considered as a system in series with the system defined by the equations of motion (1) with \mathbf{q} and $\dot{\mathbf{q}}$ as inputs and the configuration variables as outputs.

The entries in the constant coefficient matrices \mathbf{M} , \mathbf{C}_1 , \mathbf{K}_0 and \mathbf{K}_2 can be calculated from a non-minimal set of 25 bicycle parameters as described in ref.¹ A procedure for measuring these parameters for a given bicycle is described in refs^{18,19,21} whereas measured values for the bicycles used in this study are listed in Table 6 of the appendix. To determine the stability of the straight-ahead steady motion, exponential motions of the form $\mathbf{q} = \mathbf{q}_0 \exp(\lambda t)$ are assumed. Then with (1) the characteristic equation

$$\det(\mathbf{M}\lambda^2 + v\mathbf{C}_1\lambda + g\mathbf{K}_0 + v^2\mathbf{K}_2) = 0 \quad (5)$$

can be formed and the eigenvalues, λ , can be calculated, see Figure 4. In principle, there are up to four

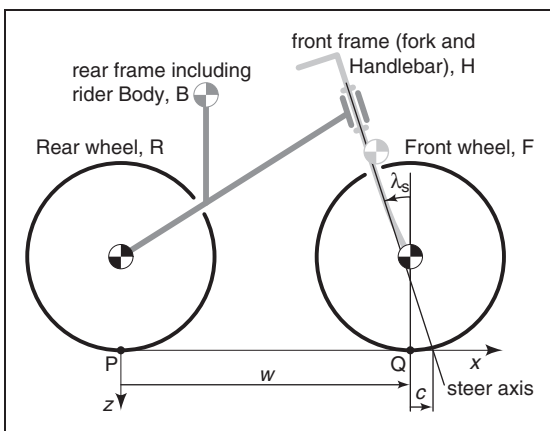


Figure 3. The bicycle model: four rigid bodies (rear wheel R, rear frame B, front handlebar assembly H, front wheel F) connected by three revolute joints (rear hub, steering axis, front hub), together with the coordinate system.

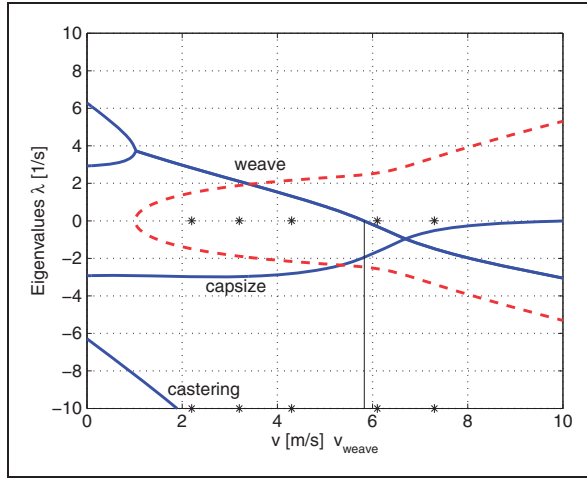


Figure 4. Eigenvalues λ for the uncontrolled instrumented bicycle from Figure 1 in the forward speed range $0 < v < 10$ m/s, solid lines are the real values and dashed lines are the imaginary values. The speed where the weave motion becomes stable is $v_{\text{weave}} \approx 5.8$ m/s. Forward speeds used in the experiments are denoted by an *.

eigenmodes, where oscillatory eigenmodes come in pairs. Two are significant and are traditionally called the *capsize* mode and the *weave* mode. The capsize mode corresponds to a real eigenvalue with an eigenvector dominated by lean: when unstable, the bicycle follows a spiraling path with increasing curvature until it falls. The weave mode is an oscillatory motion in which the bicycle sways about the heading direction. The third remaining eigenmode is the overall stable *castering* mode, like in a trailing caster wheel, which corresponds to a large negative real eigenvalue with an eigenvector dominated by steering. The eigenvalues corresponding to the kinematic differential equations are all zero and correspond to changes in the rotation angles of the wheels, a constant yaw angle and a linearly increasing lateral displacement.

For control purposes it is convenient to express the bicycle equation (1) in state-space form and as a set of transfer functions. The state-space representation is then given by

$$\dot{\mathbf{x}} = \mathbf{A}\mathbf{x} + \mathbf{B}\mathbf{f} \quad (6)$$

$$\mathbf{y} = \mathbf{C}\mathbf{x} + \mathbf{D}\mathbf{f} \quad (7)$$

with the state vector $\mathbf{x} = [\phi, \delta, \dot{\phi}, \dot{\delta}]^T$, input vector $\mathbf{f} = [T_\phi, T_\delta]^T$ and output vector $\mathbf{y} = [\phi, \delta]^T$. The system matrix \mathbf{A} , input gain matrix \mathbf{B} , observer matrix \mathbf{C} and direct feed-through matrix \mathbf{D} are then given by

$$\mathbf{A} = \begin{bmatrix} -\mathbf{M}^{-1}v\mathbf{C}_1 & -\mathbf{M}^{-1}(g\mathbf{K}_0 + v^2\mathbf{K}_2) \\ \mathbf{I} & \mathbf{0} \end{bmatrix}, \quad \mathbf{B} = \begin{bmatrix} \mathbf{M}^{-1} \\ \mathbf{0} \end{bmatrix} \quad (8)$$

$$\mathbf{C} = [\mathbf{0} \ \mathbf{I}], \quad \mathbf{D} = [\mathbf{0}]$$

The state-space equations can also be expressed as a set of transfer functions $\mathbf{H}_{yf}(s)$ by making use of

$$\mathbf{y}(s) = \mathbf{H}_{yf}(s)\mathbf{f}(s), \quad \text{with } \mathbf{H}_{yf}(s) = \mathbf{C}(s\mathbf{I} - \mathbf{A})^{-1}\mathbf{B} + \mathbf{D} \quad (9)$$

where s denotes the Laplace argument. Finally, we end by introducing the reference error \mathbf{z} . Since we are interested in roll stabilization, this simply becomes $\mathbf{z} = -\phi$, resulting in the following transfer function:

$$\mathbf{z}(s) = \mathbf{H}_{zf}(s)\mathbf{f}(s), \quad \text{where } \mathbf{H}_{zf}(s) = -[0, 0, 1, 0]\mathbf{H}_{yf}(s) \quad (10)$$

Rider control model

The rider control model is assumed to be a linear feedback system in series with neuromuscular lag. The linear feedback system is usually written as

$$\mathbf{u}(s) = -\mathbf{K}(s)\mathbf{y}(s) \quad (11)$$

with the control input \mathbf{y} , control output \mathbf{u} and linear feedback gains $\mathbf{K}(s)$. In our model the rider control input is assumed to be the bicycle lean and steer angle, $\mathbf{y} = [\phi, \delta]^T$, and for the rider control output we assume steer torque only, $\mathbf{u} = [T_{\delta,u}]$. This rider control output then acts as input to the bicycle model, $\mathbf{f} = [0, 1]^T \mathbf{u}$, and by such closes the control loop. We assume only steer torque control because according to both Weir⁵ and Moore et al.⁹ the rear frame roll angle is mainly controlled by steering, and the upper body lean action is known to be ineffective for control purposes. Moreover, during the experiments the upper body lean is restrained by a harness connected rigidly to the bicycle. In addition, the knees are also connected to the bicycle frame through a set of magnets. All together, this makes it very unlikely that the rider uses control means other than the steering control. This rider contribution to the generalized steering torque will be denoted by $T_{\delta,u}$, where the subscript u indicates the rider contribution. Next we introduce a number of sensory feedback gains, which act linearly on the bicycle configuration output. In order to explore a range of potentially relevant sensory inputs we assume the rider to be capable of sensing and applying proportional, integrative, first- and second-order derivative actions. These assumptions can be modeled mathematically according to

$$K_\phi(s) = k_{\phi p} + k_{\phi i}s^{-1} + k_{\phi d}s + k_{\phi dd}s^2 \quad (12)$$

$$K_\delta(s) = k_{\delta p} + k_{\delta i}s^{-1} + k_{\delta d}s + k_{\delta dd}s^2$$

with roll angle feedback K_ϕ and steer angle feedback K_δ . The gains k with subscript p , i , d and dd indicate proportional, integral, first- and second-order derivative gains, respectively.

According to McRuer and Jex,²² the human controller is inherently limited by neuromuscular lag and time delays. Force generation of the rider arms is modeled using activation dynamics estimated for the shoulder joint,^{23,24} which yields

$$G_{nm}(s) = \frac{\omega_c^2}{s^2 + 2\zeta\omega_c + \omega_c^2} \quad (13)$$

with cutoff frequency $\omega_c = 2.17 \cdot 2\pi$ rad/s and damping coefficient $\zeta = \sqrt{2}$. This system acts as a critically damped second-order filter with a cutoff frequency equal to ω_c . Neural transmission results in time delays, which differ for visual, vestibular and muscle feedback. We simplified the time-delay models with a single effective time delay and ultimately removed it all together for successful numerical identification as explained in the ‘Gray box model’ section. Sensory information regarding roll angle will derive from the visual and the vestibular system, while sensory information regarding steer angle will derive from muscle spindles in the arm. Manual control studies show that operators can apply proportional as well as lead (differential) or lag (integrator) control actions using visual task information.²⁵ The vestibular organ senses roll through the semicircular canals where its output is largely in phase with rotational velocity, while the otoliths sense linear acceleration, direction and magnitude of the gravitational force. The muscle spindles supply position and velocity information. The relevance, and possible sensory origin of steering angle acceleration and roll acceleration, will be addressed in the ‘Discussion’ section.

Finally, the human limitations and the linear feedback model are combined to form a rider control model according to

$$\mathbf{K}(s) = G_{nm}(s)G_\tau(s) [K_\phi(s) \quad K_\delta(s)]^T \quad (14)$$

which is presented as a block diagram in Figure 5. Note that the forward speed v serves as a parameter, such that all results depend on this since the dynamics of the bicycle is strongly forward speed dependent.

System identification

The rider control system identification uses a combination of black box and gray box models to identify the

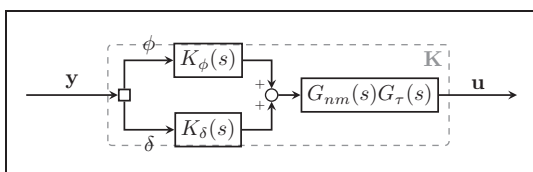


Figure 5. Block diagram of the inner control structure of \mathbf{K} , with roll and steering angle feedback gains K_ϕ and K_δ , time delay G_τ , neuromuscular lag G_{nm} , input $\mathbf{y} = [\phi, \delta]^T$ and output $\mathbf{u} = [T_{\delta,u}]^T$.

numerical values of the gains employed by the rider during each run. Starting with the basic measurements, the identification is performed in six steps:

1. Data preparation: The mean was subtracted from the roll and steer angles and the linear drift was subtracted from the lateral force.
2. Black box identification: FIR models are fit to both the lateral force and steer angle measurement pair and the lateral force and roll angle measurement pair for each run.
3. Simulation: A simulated response of roll angle and steer angle is generated by driving the FIR models with the measured lateral force.
4. Filtering: These simulated responses are then filtered to produce an idealized time history of the underlying linear relationship between the input and output.
5. Gray box identification: A gray box model structured around the feedback laws in (12) and the Whipple bicycle model is fit to the measured lateral force and the filtered response of the FIR model for each run.
6. Parameter reduction: We then reduce the parameters of the gray box model through an iterative reduction technique based on the covariance of the identified gray box parameters and the Variance Accounted For (VAF) in the lateral force to steer angle fit.

The analysis is performed for a number of forward speeds, resulting in a set of parametric models, one for each run. The accompanying data and the source code which details these methods are available for download from ref.²⁶

For the system identification a linear input/output model with additive random noise, i.e. output error, is assumed. Such a system can be described by

$$y(t) = G(q)w(t) + v(t) \quad (15)$$

with output $y(t)$, input $w(t)$, disturbance $v(t)$ and model $G(q)$, see Figure 6. The q operator acts as a discrete shifting function, such that $q^{-k}w(t) = w(t - k)$. This is a convenient description, because it separates the deterministic input related contribution $G(q)w(t)$ from the stochastic contribution $v(t)$.

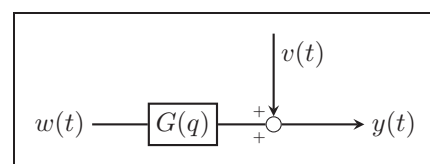


Figure 6. System description with: output $y(t)$, input $w(t)$, disturbance $v(t)$ and system $G(q)$.

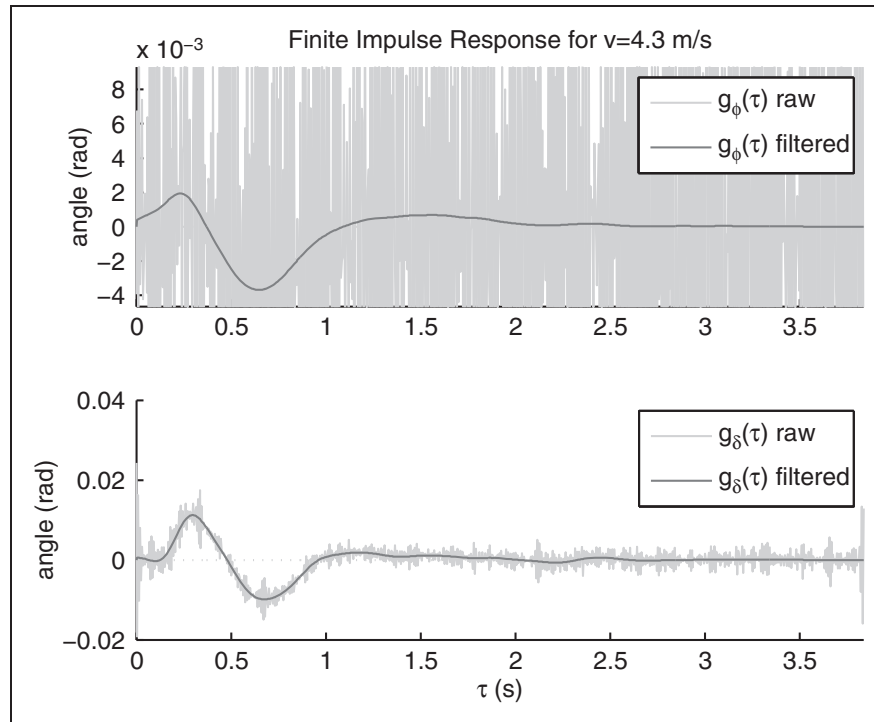


Figure 7. FIRs for the roll angle ϕ (top) and steering angle δ (bottom) for a forward velocity of $v = 4.3$ m/s (run 252). The raw FIR output is smoothed using a zero-phase low pass filter with a cutoff frequency of 10 Hz.

FIR: finite impulse response.

FIR model

Each run contains multiple perturbations in left and right directions with slightly different amplitudes, shapes and intervals. For each run an FIR model is used to capture the full system response to an applied force perturbations, and to separate it into linear deterministic and stochastic noise components. The unknown coefficient of the FIR model have been estimated by using the measured input $w(t)$ and output $y(t)$ data. The output data either represents $y(t) = \phi$ corresponding to $G_\phi(q)$ or $y(t) = \delta(t)$ corresponding to $G_\delta(q)$. We assume a finite discrete normalized time; $t = 1, 2, 3, \dots, n$, such that the approximated output $\hat{y}(t)$ is

$$\hat{y}(t) = \sum_{k=1}^m \hat{g}(k)w(t-k) + v(t) \quad (16)$$

From the experiment we know that no input outside the measurement interval $\{1 < t < n\}$ is applied, which can be expressed as: $w(t) = 0$ for $t < 1$ and $t > n$. The unknown coefficients $\hat{g}(k)$ can be solved from the linear quadratic optimization problem, $\hat{\mathbf{g}} = \arg \min_{\mathbf{g}} \{(\hat{\mathbf{y}} - \mathbf{y})^2\}$. After experimenting with different finite impulse lengths, the oscillations are found to die out after about $m = 768$ samples, which correspond to a finite response length of 3.84 s. Once the m coefficients are identified for each run the resulting FIR model is used to generate the linear outputs, ϕ and δ from the measured input w . These simulated

outputs are smoothed by applying a zero-phase low pass eighth-order Butterworth filter with a cutoff frequency of 10 Hz. The results for $v = 4.3$ m/s are shown in Figure 7.

Noise

We can use the FIR model to estimate the noise or remnant $v(t)$, from (15), we obtain

$$\hat{\mathbf{v}}(t) = \mathbf{y}(t) - \hat{\mathbf{G}}_N(q)w(t) \quad (17)$$

where $\hat{\mathbf{v}}(t) = [v_\phi(t), v_\delta(t)]^T$ is the estimated remnant and $\hat{\mathbf{G}}_N(q) = [\hat{G}_\phi(q), \hat{G}_\delta(q)]^T$ represents the obtained impulse response model from input $w(t)$ to output $y(t)$. The decomposition of the measured data into the deterministic input related component and remnant component is shown for $v = 4.3$ m/s in Figure 8.

When inspecting the unfiltered FIR output, see Figure 7, it is apparent that the high-frequency noise is merely an artifact of the deconvolution process and does not originate from the rider/bicycle system itself. This makes the signals ideal for simple low pass filtering. A number of observations can also be made about the output error, $v(t)$, shown in Figure 8. The small amplitude changes in both the roll and steering angle about 2–3 s after the lateral perturbation do not seem to be linearly correlated with the input force and are likely due to the human induced remnant. The signal-to-noise ratio for the case $v = 2.1$ m/s (not shown here) is very low, resulting in an unreliable

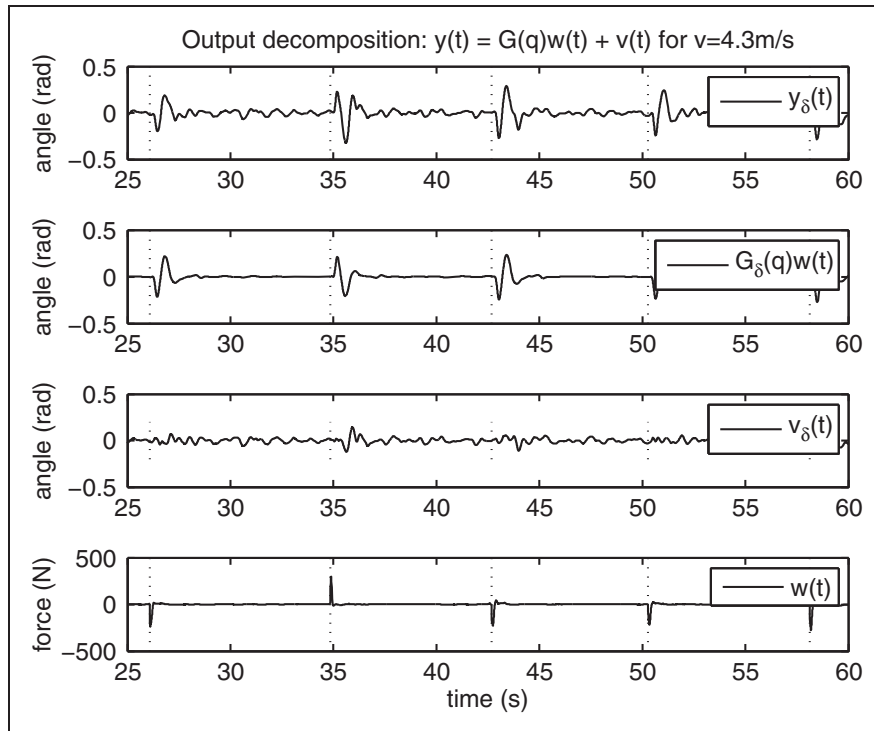


Figure 8. Output decomposition of the steering angle output $y(t)$ in terms of input related component $G(q)w(t)$ and remnant component $v(t)$ for a forward velocity of $v = 4.3$ m/s (run 252).

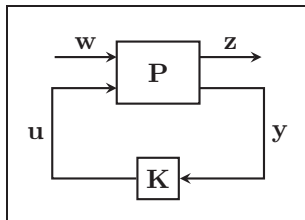


Figure 9. Block diagram of the general control description, with known bicycle dynamics P , unknown controller K , disturbance input w , error output $z = -\phi$, control input y and control output u .

FIR model. The signal-to-noise ratio of the steering angle response is generally higher than the roll angle response. The overall shape of the roll and steering angle responses are similar, but the amplitudes and time characteristics differ. The amplitudes of the output oscillations decrease as the forward velocity increases. The impulse response seems to damp out more quickly as the forward velocity increases, which may have some corollary to the open-loop dynamics of the bicycle.

Gray box model

In the rider control model, the parameters are the unknown linear feedback control gains from (12). The complete system model, the bicycle model together with the feedback control model, is shown in Figure 9. Its structure constitutes a standard

linear gray box model formulation. The corresponding gray box model structure is then given by

$$\begin{aligned} y(\theta) &= G(\theta)w, G(\theta) \\ &= \left[P_{yw} + P_{yu}(\mathbf{I} - K(\theta)P_{yu})^{-1}K(\theta)P_{yw} \right] \end{aligned} \quad (18)$$

with bicycle dynamics P_{yw} and P_{yu} , human controller $K(\theta)$ with the unknown gains k defined as the model parameters θ , disturbance input $w = w$ and output $y = [\phi, \delta]^T$. Notice that only the human controller parameters are unknown, while the open-loop bicycle parameters are known since they are determined a priori from the bicycle model (8).

The error criteria used to estimate the gray box parameters θ is based on a weighted quadratic sum

$$V_N(\theta) = \frac{1}{N} \sum_{t=1}^N \left[\left(\hat{G}_\delta(q) - G_\delta(q, \theta) \right) w(t) \right]^2 \quad (19)$$

which is different than the previous FIR error criteria by the addition of the weighting by the input signal w . This weighting forces the minimizer to positively weight the portion of the time series with higher signal-to-noise ratios. Here, we also only use the measured steering angle response because both single-input and single-output (SISO) identification is more tractable than single-input and multiple-output (SIMO) identification and, with the rider directly exciting the steering dynamics, it is expected that the steering signal contains the most direct information

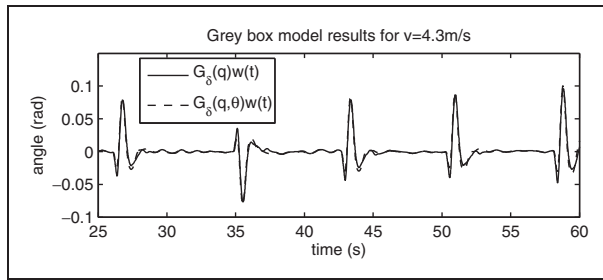


Figure 10. Comparison of the filtered FIR output, $G_{\delta}(q)$, and the identified gray box model response $G_{\delta}(q, \theta)$ of the steer angle δ , at a forward speed of $v = 4.3$ m/s (run 252). FIR: finite impulse response.

concerning rider actions. The initial parameter vector θ_0 is determined by a random search method, for which the lowest criteria score is further optimized by using the `lsqnonlin` function in Matlab. The parameter optimization results in an optimal parameter vector set according to

$$\hat{\theta} = \arg \min_{\theta} V_N(\theta) \quad (20)$$

The parameters are identified for 15 runs, where the forward velocity takes the following values, 2.1, 3.2, 4.3, 6.1 and 7.3 m/s, with multiple runs per speed, see Table 1. Numerical issues and instabilities in the identification process were encountered with the rider model with a time delay. For the current study, this problem is circumvented by ignoring the time delay and setting it to zero. This ultimately affects the identified values of the controller gains but does so equally for each run, thus maintaining the ability to compare parameter values among runs.

As an example, the resulting response from the gray box model for a forward velocity of $v = 4.3$ m/s is shown in Figure 10. The comparison of this model response to the FIR model is shown in Figure 11.

The gray box model, with its eight free parameters, adequately fits the data for each run but the identified parameters were susceptible to over-fitting due to the a priori structure of the model and it was likely that some of the feedback gains were not necessarily employed by human riders. Hence, to determine the essential feedback loops in the rider control system we apply a parameter reduction technique. The reduction is based on the quality of the fit and selection of parameters guided by the parameter covariance as defined by Ljung.²⁷ The quality of the fit is measured by the VAF on the deterministic output $y_d(t)$, which is defined as the normalized difference between the gray box model response and the filtered FIR model response

$$\text{VAF}(\theta) = 1 - \frac{\sum_{t=1}^n (e(t, \theta))^2}{\sum_{t=1}^n (y_d(t))^2}, \quad \text{with } e(t, \theta) = y_d(t) - \hat{y}_d(t, \theta) \quad (21)$$

with the deterministic output defined as the output minus the output error (i.e. the noise), as in

$$y_d(t) = y(t) - v(t) = G(q)w(t) \quad (22)$$

A VAF score of 1 means a perfect fit. The sensitivity of the quality of the fit with respect to the parameters θ is defined by the parameter covariance

$$\text{cov}_{\theta_{ij}} = \rho \left[\frac{1}{n} \sum_{t=1}^n \psi(t, \theta_i) \psi(t, \theta_j) \right]^{-1}, \quad \text{with } \rho = \frac{1}{n} \sum_{t=1}^n [e(t, \theta)]^2 \quad (23)$$

and with the partial derivative of the error $e(t, \theta)$ with respect to the i th parameters θ_i defined as

$$\psi(t, \theta_i) = -\frac{d}{d\theta_i} e(t, \theta) = \frac{d}{d\theta_i} \hat{y}_d(t, \theta) \quad (24)$$

A reduced model with a minimal set of parameters was derived as follows. Instead of calculating all $8! = 40,320$ possible combinations of contributing feedback parameters, we start from a full parameter set and guided by the parameter covariance remove the parameter which has the least influence on the quality of the fit. This process is repeated until the quality of the fit drops below a certain threshold, e.g. 90%. An example of this parameter reduction process, for $v = 4.3$ m/s, is shown in Figure 12, whereas the results for three forward speeds (low, mid and high), are presented in Table 2. As a first observation it is clear that not all feedback control gains are important, in most cases at least four out of the initial eight parameters can be omitted. The remaining parameters are a proportional and differential feedback on the roll angle and an integral and differential gain on the steer angle, where the integrated steering angle reflects the heading error. These results and implications will further be discussed in detail in the ‘Discussion’ section.

Finally, we check the stability of the rider controlled system by calculating the eigenvalues for the closed-loop system with the set of reduced control model parameters, where these results are presented in Table 3. We observe that the number of state variables has increased from 4 to 7. Two states are added due to the neuromuscular activation dynamics G_{nm} , which acts as a second-order low pass filter on the controller output and one state is added due to the integrative feedback action on the steering angle. The real parts of all eigenvalues are negative, which indicates that the closed-loop system is indeed stable. If we compare these results to the open-loop uncontrolled dynamics, as represented by the eigenvalues from Figure 4, we see that unstable roots at forward speeds $v = 2.2$, $v = 3.2$ and $v = 4.3$ m/s are clearly stabilized.

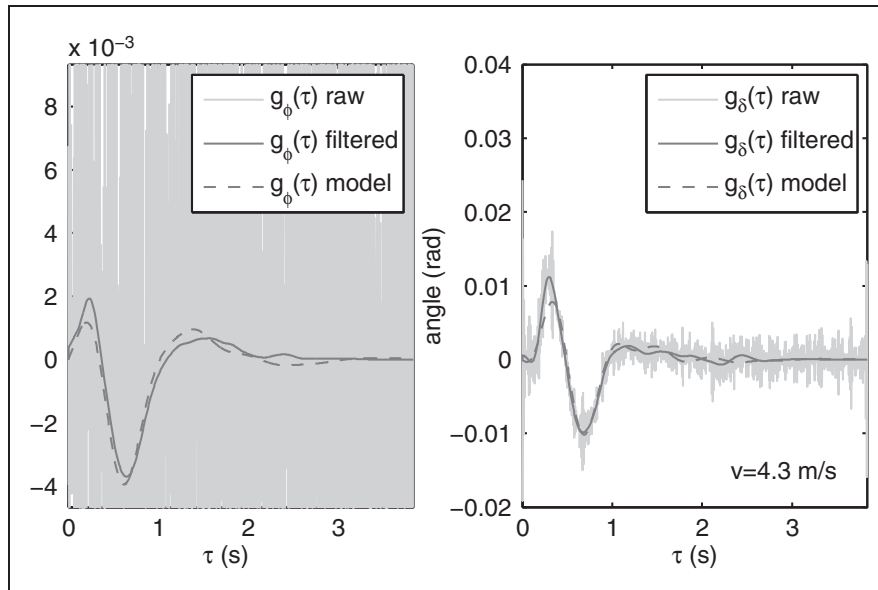


Figure 11. Zoomed in comparison of the FIR output, the filtered FIR output, and the gray box response of lean angle ϕ (left) and the steer angle δ (right), at a forward speed of $v = 4.3$ m/s (run 252).
FIR: finite impulse response.

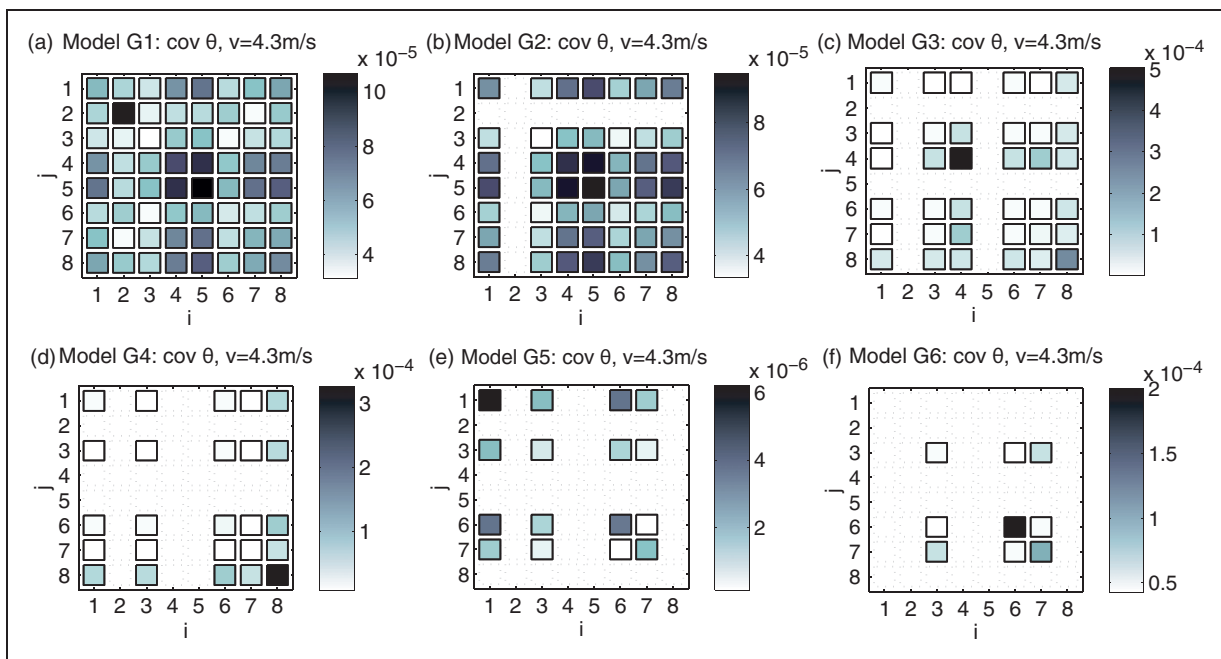


Figure 12. Example of subsequent parameter covariance matrices after iterative parameter reduction for run 252 which is at a forward velocity of $v = 4.3$ m/s, where darker shading means higher covariance and lower sensitivity. The parameter space is reduced by one for each iteration by removing the gain which has the highest covariance (dark square), from G1 to G6 until the VAF value drops down dramatically. The subsequent VAF values are: (99.36, 98.92, 96.75, 96.39, 95.18, 63.49)%.
VAF: Variance Accounted For.

Optimal control approach

Here, we attempt to address the question: ‘if the rider is operating like an optimizer then what is the rider optimizing?’ To answer this question we formulate a standard LQR optimal control problem²⁸ with the performance index (or cost function) for the

control task

$$J = \int (\mathbf{x}^T \mathbf{Q} \mathbf{x} + \mathbf{u}^T \mathbf{R} \mathbf{u}) dt \tag{25}$$

with the state vector $\mathbf{x} = (\dot{\phi}, \delta, \phi, \delta, \int \delta)$ and the controller output $\mathbf{u} = (\tau_{\delta})$, and the weight factors \mathbf{Q} on

Table 2. Overview of gray box model identification results, with controller \mathbf{K} , parameter vector θ , forward velocity v (m/s), roll proportional gain $k_{\phi p}$ (Nm/rad), roll integrative gain $k_{\phi i}$ (Nm/s rad), roll derivative gain $k_{\phi d}$ (Nm s/rad), roll 2nd derivative gain $k_{\phi dd}$ (Nm s²/rad), steer proportional gain $k_{\delta p}$ (Nm/rad), steer integrative gain $k_{\delta i}$ (Nm/s rad), steer derivative gain $k_{\delta d}$ (Nm s/rad), steer 2nd derivative gain $k_{\delta dd}$ (Nm s²/rad) and Variance Accounted For (VAF) (%). The gray marked rows indicate the reduced models which have a minimal number of parameters and still show a good fit (VAF > 90 %). As an example the covariance matrices of these reduction steps for run 252 ($v = 4.3$ m/s) are depicted in Figure 12.

Model	$k_{\phi p}$	$k_{\phi i}$	$k_{\phi d}$	$k_{\phi dd}$	$k_{\delta p}$	$k_{\delta i}$	$k_{\delta d}$	$k_{\delta dd}$	VAF
Run 249: $\mathbf{K}(s, \theta(v = 2.2))$	288.08	-100.30	93.86	-5.80	-23.43	186.05	-9.61	-0.50	99.26
	265.93		96.81	-6.56	-23.91	162.90	-10.36	-0.51	99.09
	59.65		47.50	-0.27		56.74	-3.36	-0.11	98.73
	56.15		44.66			53.20	-3.05	-0.09	98.72
	28.97		32.85			29.02	-2.50		94.89
			27.68			5.45	-2.39		80.82
			27.73				-2.60		79.59
		27.98						0.00	
Run 252: $\mathbf{K}(s, \theta(v = 4.3))$	265.18	-239.20	108.92	-8.09	-98.47	957.34	-20.61	-0.79	99.36
	269.35		108.24	-9.63	-124.76	812.04	-23.90	-0.81	98.92
	50.84		38.90	-0.43		258.14	-4.59	-0.08	96.75
	51.01		34.23			231.07	-3.62	-0.08	96.39
	41.51		28.22			177.45	-3.19		95.18
			21.47			22.08	-3.52		63.49
			21.37				-3.86		62.44
		20.59						0.00	
Run 256: $\mathbf{K}(s, \theta(v = 7.3))$	260.06	-240.71	90.53	-6.67	-303.87	2272.89	-35.13	-0.59	96.94
	279.86		85.17	-7.27	-356.87	1869.45	-37.61	-0.63	96.32
	54.82		40.80	-0.35		791.19	-10.84	-0.03	90.41
	51.84		40.61	-0.45		769.67	-11.20		90.32
	48.65		29.89			583.43	-7.05		90.09
			16.90			26.54	-6.64		61.82
			16.73				-6.94		61.24
		16.34						0.00	

VAF: Variance Accounted For.

Table 3. Feedback control gains $\mathbf{K}(12)$ of the reduced parameter rider control model and eigenvalues λ for the corresponding closed-loop control system, with experiment identification number id, forward velocity v , and VAF, for a rider model with no time delay $\tau_d = 0$.

id	v m/s	$k_{\phi p}$ Nm/rad	$k_{\phi d}$ Nm/s rad	$k_{\delta i}$ Nm/rads	$k_{\delta d}$ Nm/s rad	VAF %	λ_1 rad/s	$\lambda_{2,3}$ rad/s	$\lambda_{4,5}$ rad/s
248	2.1	5.17	27.21	14.39	-1.92	85	-18.11	$-0.90 \pm 3.26i$	$-0.67 \pm 1.70i$
249	2.2	28.97	32.85	29.02	-2.50	95	-21.33	$-1.54 \pm 1.85i$	$-0.39 \pm 3.33i$
250	2.2	24.25	32.51	26.44	-2.57	96	-21.82	$-1.41 \pm 1.90i$	$-0.46 \pm 3.18i$
184	3.2	22.72	26.12	65.92	-3.00	95	-26.76	$-1.42 \pm 3.13i$	$-0.66 \pm 3.08i$
185	3.2	43.23	30.45	94.00	-3.21	97	-27.58	$-2.15 \pm 2.43i$	$-0.30 \pm 3.92i$
186	3.1	31.12	28.46	71.26	-2.95	97	-26.05	$-1.50 \pm 2.68i$	$-0.77 \pm 3.64i$
251	4.3	72.83	32.44	211.79	-3.81	90	-33.45	$-2.54 \pm 1.83i$	$-0.73 \pm 5.50i$
252	4.3	41.51	28.22	177.45	-3.19	95	-29.82	$-1.94 \pm 3.37i$	$-1.18 \pm 4.18i$
253	4.3	45.43	28.99	169.47	-3.60	95	-32.49	$-1.75 \pm 2.68i$	$-1.20 \pm 4.79i$
190	6.0	34.19	23.34	334.82	-3.52	97	-36.60	$-2.35 \pm 4.65i$	$-1.17 \pm 3.84i$

(continued)

Table 3. Continued

id	v m/s	$k_{\phi\phi}$ Nm/rad	$k_{\phi d}$ Nm/s/rad	$k_{\delta i}$ Nm/rads	$k_{\delta d}$ Nm/s/rad	VAF %	λ_1 rad/s	$\lambda_{2,3}$ rad/s	$\lambda_{4,5}$ rad/s
191	6.1	29.63	22.83	322.89	-3.81	96	-38.82	$-2.47 \pm 5.02i$	$-0.87 \pm 3.46i$
192	6.1	28.32	20.43	293.30	-3.31	92	-36.00	$-2.16 \pm 4.79i$	$-1.09 \pm 3.60i$
255	7.3	37.19	26.66	533.49	-5.37	92	-51.53	$-2.73 \pm 6.55i$	$-1.08 \pm 2.95i$
256	7.3	48.65	29.89	583.43	-7.05	90	-61.74	$-2.10 \pm 6.56i$	$-1.48 \pm 2.71i$
257	7.4	45.58	26.97	617.10	-4.64	93	-46.73	$-2.56 \pm 5.97i$	$-1.70 \pm 3.47i$

VAF: Variance Accounted For.

the state and \mathbf{R} on the control effort. The optimal feedback gains \mathbf{K} for a linear feedback controller of the form $\mathbf{u} = -\mathbf{K}\mathbf{x}$ are found by minimizing the performance index J , which is done with the well-known Riccati solution (LQR model). Here, we work the other way around: given the feedback gains from the reduced parameter rider model (Table 3), what are the weight factors? We solve this by a nonlinear search on J . For the weight factors we take the same approach as used by Bryson and Ho,²⁸ where we assume all off-diagonal terms in \mathbf{Q} and \mathbf{R} zero, and the remaining unknown diagonal terms to have the form $1/\hat{x}_i^2$, where \hat{x}_i is the maximal allowable value of the i th element of the state vector. The weight factor matrices \mathbf{Q} and \mathbf{R} then take on the form

$$\mathbf{Q} = \text{diag}(1/\hat{\phi}^2, 1/\hat{\delta}^2, 1/\hat{\phi}^2, 1/\hat{\delta}^2, 1/\hat{\psi}^2) \quad (26)$$

$$\mathbf{R} = 1/\hat{\tau}_\delta^2 \quad (27)$$

To obtain more meaningful results we have introduced the approximate maximum allowable heading angle $\hat{\psi} = v \cos \lambda_s/w \int \delta dt$ as a physical interpretation of the state variable $\int \delta dt$. This approximate heading follows directly from the kinematic equation (2), when we neglect the small contribution of the trail times steer rate term. The unknown weight factors are now the maximum allowable state variables $(\hat{\phi}, \hat{\delta}, \hat{\phi}, \hat{\delta}, \hat{\psi})$ and the maximum allowable steer torque $\hat{\tau}_\delta$. These weight factors are found in an optimization process by minimizing the absolute difference between the feedback control gains from the reduced parameter model and the ones from the corresponding LQR method. To simplify matters, the neuromuscular lag G_{nm} and time delay G_τ in the feedback model 14 have been neglected. The justification is that this system acts as a second-order filter at a cutoff frequency of 2.17 Hz, whereas the observed control signals are in the order 1 Hz.

The results of this process are the \mathbf{Q} and \mathbf{R} weight factors shown in Table 4 and Figure 14, together with the approximate feedback control gains shown in Table 5 and added to Figure 13. Instead of the four feedback gains from the reduced parameter model we now have five feedback gains because the LQR

method used here has full state feedback. The weight factors are normalized with respect to the control effort, that is normalized with $\tau_\delta = 1$. Clearly, looking at the weights in Table 4, the rider is not optimizing with respect to the roll or steer angle or rates, indicated by the high maximum allowable values. At low speed ($v < 3$ m/s), the rider is optimizing the control effort, since here the smallest values are the maximum allowable steer torques. At moderate to high speed, the rider is optimizing for heading, indicated by the small value (negative number on a log scale) of the maximum allowable heading $\hat{\psi}$, which makes sense when balancing a moving bicycle on a narrow treadmill.

Discussion

Identified parameter values for the linear feedback rider control model according to Figure 5 and equation (12), for all five forward speeds, are presented in Table 3 and Figure 13, from which the following observations can be made. The reduced gray box model with four feedback gains accounts for 90% of the variance of the FIR model output, see Table 2 and Figure 12. These four gains are: a gain on the lean angle and lean rate and a gain on the steer rate and the integral of the steer angle. The rider's use of lean angle and lean angle rate represents vestibular and/or visual feedback, and the use of steer angle rate represents proprioceptive feedback. The sign of the gains on the lean angle and lean angle rate are in total agreement with the basic bicycle balance principle of steer-into-the-fall.² The feedback of the integral of the steer angle can be explained by the need for the rider to stay on the narrow treadmill and thus maintain a tight heading because the heading ψ is mainly determined by the integral of the steer angle δ , according to the kinematic equation (2). All feedback gains show a forward speed dependency, the most profound in the integral steering feedback (heading), which seems to be quadratic in the forward speed.

To understand what the rider is optimizing we have successfully applied the LQR method in an inverse manner. The resulting weight factors, in Table 4 and Figure 14 indicate that at low speed ($v < 3$ m/s) the rider is minimizing his control effort and at high speed

Table 4. \log_{10} of the weight factors ($\hat{\phi}, \hat{\delta}, \hat{\phi}, \hat{\delta}, \hat{\psi}$) for the state vector weight matrix Q , together with the experiment identification number id , forward velocity v and performance index or cost function J . The heading weight factor $\hat{\psi}$ is a measure for the weight on the integral of the steer angle. The weights are normalized with respect to the control effort R , setting $\hat{\tau}_\delta = 1$ ($\log_{10}(\hat{\tau}_\delta) = 0$). Clearly run 191 and 255 are outliers, because of the high value of J compared to the other runs.

id	v m/s	Q					J –
		$\log \hat{\phi}$ rad/s	$\log \hat{\phi}$ rad	$\log \hat{\delta}$ rad/s	$\log \hat{\delta}$ rad	$\log \hat{\psi}$ rad	
248	2.1	2.3	3.6	2.5	2.5	3.3	1939
249	2.2	5.6	6.9	5.9	6.8	–0.9	1520
250	2.2	–1.2	2.1	1.6	2.0	2.2	1510
184	3.2	6.5	7.1	5.8	7.3	–2.0	2376
185	3.2	5.2	5.4	3.7	4.1	–2.3	2664
186	3.1	6.3	6.7	5.5	6.0	–2.1	2317
251	4.3	–1.0	0.4	–0.7	–0.3	–2.9	2590
252	4.3	5.9	6.2	5.3	5.6	–2.8	3539
253	4.3	3.5	4.1	3.7	3.7	–2.8	2795
190	6.0	5.1	6.0	4.9	5.3	–3.3	3939
191	6.1	–0.6	0.6	–1.7	–2.0	–3.2	19153
192	6.1	5.6	6.3	5.1	5.5	–3.2	3316
255	7.3	–1.0	–0.3	–2.0	–1.7	–3.5	16352
256	7.3	4.8	6.0	4.5	4.7	–3.6	3601
257	7.4	4.8	5.6	4.3	4.2	–3.6	4492

Table 5. Feedback control gains $K(12)$ obtained from the optimal control approach with experiment identification number id , forward velocity v , performance index or cost function $J(25)$ and no time delay $\tau_d = 0$. The optimal criterion weights Q and R are presented in Table 4. For comparison with the original reduced parameter model gains these values are plotted as * in Figure 13. Clearly run 191 and 255 are outliers, because of the high value of J compared to the other runs.

id	v m/s	$k_{\phi p}$ Nm/rad	$k_{\phi d}$ Nm/s/rad	$k_{\delta p}$ Nm/rad	$k_{\delta i}$ Nm/rads	$k_{\delta d}$ Nm/s/rad	J –
248	2.1	41.18	14.50	–16.55	0.00	–1.79	1939
249	2.2	47.31	16.58	–16.34	3.50	–1.82	1520
250	2.2	43.31	21.55	–18.10	0.00	–2.00	1510
184	3.2	56.86	19.54	–17.32	36.50	–1.86	2376
185	3.2	81.10	27.82	–15.60	62.72	–2.01	2664
186	3.1	64.74	22.26	–16.73	41.81	–1.91	2317
251	4.3	115.19	40.56	–16.79	190.68	–2.44	2590
252	4.3	93.14	31.60	–16.73	153.35	–2.17	3539
253	4.3	90.82	30.81	–16.99	148.48	–2.16	2795
190	6.0	90.98	30.35	–22.00	321.40	–2.30	3939
191	6.1	125.80	38.97	–76.44	261.24	–3.85	19,153
192	6.1	79.20	26.31	–23.44	281.37	–2.18	3316
255	7.3	147.21	39.55	–52.95	497.79	–3.58	16,352
256	7.3	102.18	33.76	–25.26	575.53	–2.50	3601
257	7.4	106.61	35.27	–24.70	607.93	–2.55	4492

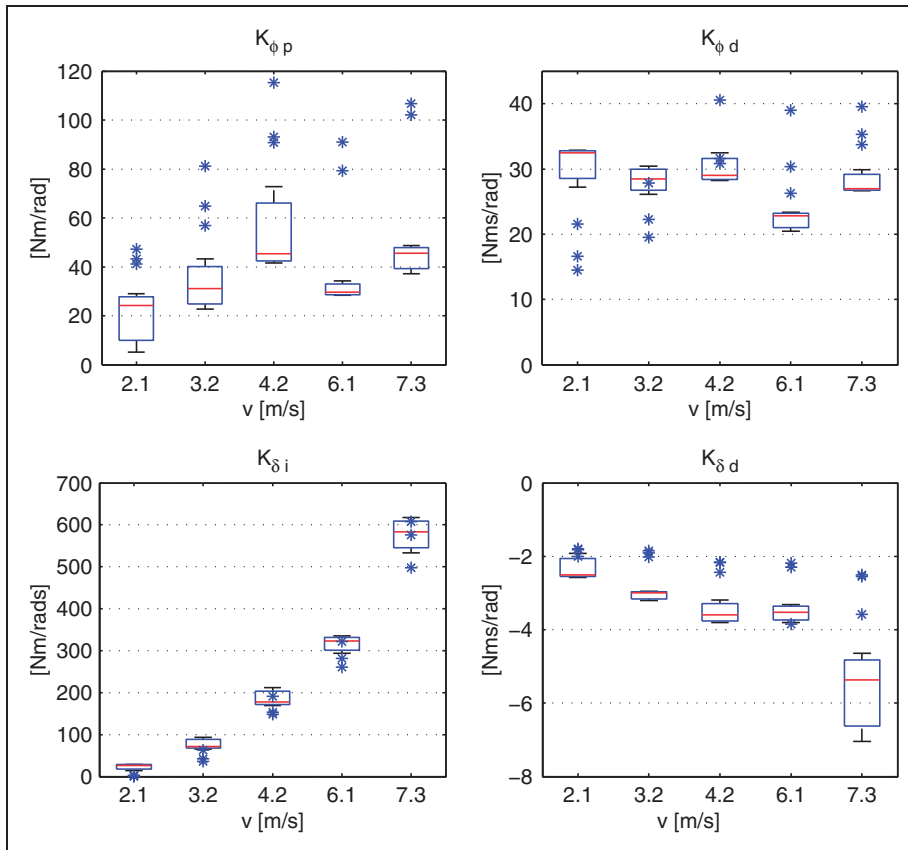


Figure 13. Box plot of the feedback control gains $K(12)$ of the reduced parameter rider control models from Table 3, as a function of the forward velocity v , together with the feedback control gains obtained by the optimal control approach from Table 5, which are marked by an *.

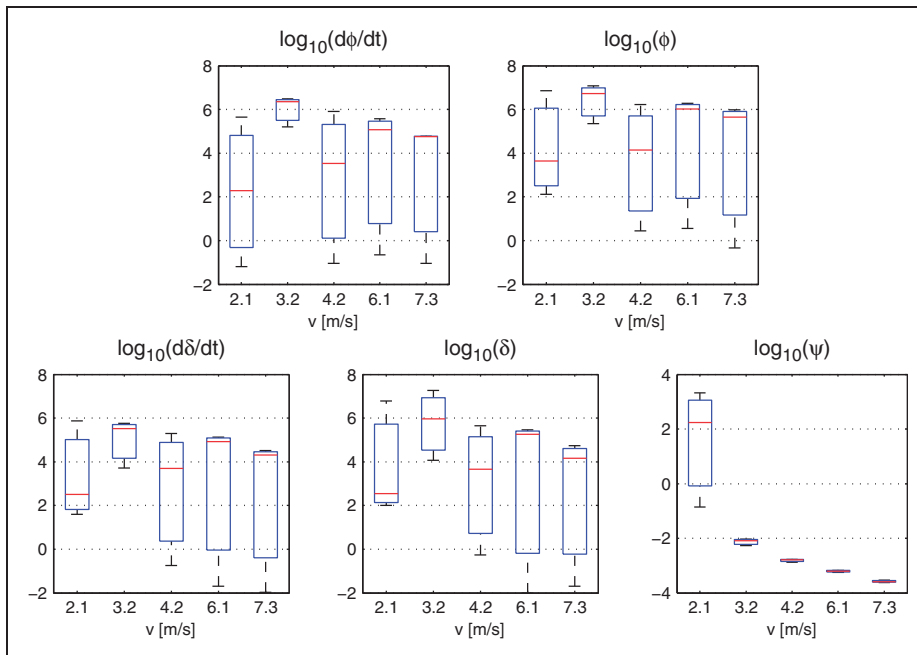


Figure 14. Box plot of the \log_{10} of the maximum allowable state variable values ($\hat{\phi}, \hat{\delta}, \hat{\dot{\phi}}, \hat{\dot{\delta}}, \hat{\psi}$) from Table 4, which are used in the optimal control state vector weight matrix Q , as a function of the forward velocity v . Note that the weights are normalized with respect to the control effort R , setting $\hat{v}_{\delta} = 1$ ($\log_{10}(\hat{v}_{\delta}) = 0$).

he is minimizing his heading error. The weight factors on the heading show a strong forward speed dependency, all other factors do not. The resulting control feedback gains comply pretty well with the original feedback gains from the reduced order model, as can be seen in Figure 13. The proportional feedback on the roll angle are about twice as high and the feedback on the steer rate, which can be seen as some sort of steer damping, show the same forward speed dependency but stay a bit behind, which can be attributed to the neglected human muscular dynamics. The feedback gain on the integral of the steer angle, the approximate heading, complies very well.

Conclusion

Rider control in bicycling is identified by a linear feedback control model where muscle dynamics are incorporated. The measured data were obtained while riding on a narrow treadmill where the system was perturbed by an intermittent lateral impulsive force. The identified rider control model with the reduced parameter set stabilizes the system, follows the necessary stability condition of steer into the fall and seems to mimic human control in a natural way. Application of optimal control theory on the identified rider control model indicates that at low speed the rider minimizes his control effort and at high speed he minimizes the heading error. This seems very plausible for the task of riding on a narrow treadmill. Future research will be conducted to obtain experimental data of bicycling on the open road, where the restriction of keeping a narrow lane, like on the treadmill, is not imposed. The same techniques as described in this article can then be used to obtain a pure stabilizing rider control model.

Funding

This material is partially based upon work supported by the National Science Foundation under Grant No. 0928339. Any opinions, findings, and conclusions or recommendations expressed in this material are those of the author(s) and do not necessarily reflect the views of the National Science Foundation.

Conflict of interest

None declared.

Acknowledgments

We thank Andy Ruina for asking the question on what the rider is optimizing and to all of the assistants who helped develop the instrumented bicycle and run the experiments.

References

1. Meijaard JP, Papadopoulos JM, Ruina A, et al. Linearized dynamics equations for the balance and steer of a bicycle: a benchmark and review. *Proc R Soc A* 2007; 463: 1955–1982.
2. Kooijman JDG, Meijaard JP, Papadopoulos JP, et al. A bicycle can be self-stable without gyroscopic or caster effects. *Science* 2011; 332: 339–342.
3. A. van Lunteren and H. G. Stassen. On the variance of the bicycle rider's behavior. In: *Proceedings of the 6th annual conference on manual control*. Air Force Institute of Technology Air Force Flight Dynamics Laboratory Wright Patterson AFB, Ohio, 7–9 April 1970.
4. RS. Rice and R Roland. *An evaluation of the performance and handling qualities of bicycles*. Technical Report, Cornell Aero. Lab. Rept. VJ-2888-K, April 1970, <http://bicycle.tudelft.nl/schwab/Bicycle/calspan/>
5. DH. Weir. *Motorcycle handling dynamics and rider control and the effect of design configuration on response and performance*. PhD Thesis, University of California, LA, 1972.
6. D.J. Eaton. *Man-machine dynamics in the stabilization of single-track vehicles*. PhD Thesis, University of Michigan, 1973.
7. Sharp RS. The stability and control of motorcycles. *J Mech Eng Sci* 1971; 13(5): 316–329.
8. Popov AA, Rowell S and Meijaard JP. A review on motorcycle and rider modelling for steering control. *Veh Syst Dyn* 2010; 48: 775–792.
9. Moore JK, Kooijman JDG, Schwab AL, et al. Rider motion identification during normal bicycling by means of principal component analysis. *Multibody Syst Dyn* 2011; 25(2): 225–244.
10. Hess R, Moore JK and Hubbard M. Modeling the manually controlled bicycle. *IEEE Trans Syst Man Cybern, Part A: Syst Humans* 2011; (99): 1–13.
11. McRuer DT, Graham D and Krendel ES. Manual control of single-loop systems: part i. *J Franklin Inst* 1967; 283(1): 1 – 29.
12. McRuer DT, Graham D and Krendel ES. Manual control of single-loop systems: part ii. *J Franklin Inst* 1967; 283(2): 145–168.
13. McRuer DT, Allen RW, Weir DH, et al. New results in driver steering control models. *Human Factors: J Human Factors Ergonom Soc* 1977; 19(4): 381–397.
14. A. J. R. Doyle. *The skill of bicycle riding*. PhD Thesis, University of Sheffield, UK, 1987, <http://bicycle.tudelft.nl/schwab/Bicycle/doyle1987skill.pdf>.
15. J. Milton, J.L. Cabrera, T. Ohira, et al. The time-delayed inverted pendulum: Implications for human balance control. *Chaos: Interdis J Nonlinear Sci* 19:026110, 2009.
16. A. L. Schwab, P. D. L. de Lange, R. Happee, et al. Rider control identification in bicycling, parameter estimation of a linear model using lateral force perturbation tests. In: *Proceedings of the IMSD2012 – The 2nd joint international conference on multibody system dynamics*, 29 May 29 – 1 June 2012 Stuttgart, Germany, 2012, pp. 1–16.
17. <http://biosport.ucdavis.edu/research-projects/bicycle/instrumented-bicycle> .
18. JK. Moore. *Human control of a bicycle*. PhD Thesis, University of California Davis, CA, 2012.
19. J. K. Moore, M. Hubbard, J. D. G. Kooijman, et al. A method for estimating physical properties of a combined bicycle and rider. In: *Proceedings of the ASME 2009 international design engineering technical conferences & computers and information in engineering*

- conference, *DETC2009*, San Diego, CA, 30 Aug–2 Sep 2009, 2009.
20. F. J. W. Whipple. The stability of the motion of a bicycle. *Q J Pure Appl Math* 30:312–348, 1899.
 21. Kooijman JDG, Schwab AL and Meijaard JP. Experimental validation of a model of an uncontrolled bicycle. *Multibody Syst Dyn* 2008; 19: 115–132.
 22. McRuer DT and Jex H.R. A review of quasi-linear pilot models. *IEEE Trans Human Factors Electron HFE*-1967; 8(3): 231–249.
 23. de Vlugt E, Schouten AC and van der Helm FCT. Closed-loop multivariable system identification for the characterization of the dynamic arm compliance using continuous force disturbances: a model study. *J Neurosci Methods* 2003; 122(2): 123–140.
 24. Happee R, De Vlugt E and Schouten AC. Posture maintenance of the human upper extremity; identification of intrinsic and reflex based contributions. *SAE Int J Passenger Cars-Mech Syst* 2009; 1(1): 1125.
 25. D. T. McRuer and E. S. Krendel. *Dynamic response of human operators*. Technical Report WADC-TR-56-524, Wright Air Development Center, Oct. 1957.
 26. P.D.L. de Lange and Jason K. Moore. *Bicycle rider control identification source code and data*, <http://dx.doi.org/10.6084/m9.figshare.659465> (2013).
 27. L. Ljung. *System identification: theory for the user*. Englewood Cliffs, NJ: Prentice-Hall 1987.
 28. Bryson AE and Ho YC. *Applied optimal control*. New York: Wiley, 1975.

Appendix: Bicycle parameters

Table 6. Parameters for the measurement bicycle plus rigid rider from Figure 1 for the bicycle model from Figure 3.

Parameter	Symbol	Values
Wheel base	w	1.0759 m
Trail	c	0.0718 m
Steer axis tilt	λ_s	20.1°
Gravity	g	9.81 N/kg
Forward speed	v	various m/s
Rear wheel R		
Radius	r_R	0.3325 m
Mass	m_R	4.90 kg
Inertia	(I_{Rxx}, I_{Ryy})	(0.0701, 0.12934) kg m ²
Rear Body and frame assembly B		
Centre of mass	(x_B, z_B)	(0.33235, -1.02217) m
Mass	m_B	106.40 kg
Inertia	$\begin{bmatrix} I_{Bxx} & 0 & I_{Bxz} \\ 0 & I_{Byy} & 0 \\ I_{Bxz} & 0 & I_{Bzz} \end{bmatrix}$	$\begin{bmatrix} 13.9967 & 0 & -0.6113 \\ 0 & 15.4633 & 0 \\ -0.6113 & 0 & 4.4282 \end{bmatrix}$ kg m ²
Front Handle bar and fork assembly H		
Centre of mass	(x_H, z_H)	(0.8092, -0.9774) m
Mass	m_H	5.40 kg
Inertia	$\begin{bmatrix} I_{Hxx} & 0 & I_{Hxz} \\ 0 & I_{Hyy} & 0 \\ I_{Hxz} & 0 & I_{Hzz} \end{bmatrix}$	$\begin{bmatrix} 0.3376 & 0 & -0.0996 \\ 0 & 0.3399 & 0 \\ -0.0996 & 0 & 0.1094 \end{bmatrix}$ kg m ²
Front wheel F		
Radius	r_F	0.3356 m
Mass	m_F	1.55 kg
Inertia	(I_{Fxx}, I_{Fyy})	(0.0524, 0.0984) kg m ²

Table 7. Mass, damping and stiffness matrices (l) for the bicycle model from Figures 3 and 1 according to the parameters from Table 6, together with the transfer matrix \mathbf{H}_{fw} which maps the lateral force applied at the seat post to the generalized forces from the bicycle model.

$$\mathbf{M}_0 = \begin{bmatrix} 133.31668525 & 2.43885691 \\ 2.43885691 & 0.22419262 \end{bmatrix}, \quad \mathbf{C}_1 = \begin{bmatrix} 0 & 44.65783277 \\ -0.31500940 & 1.46189246 \end{bmatrix},$$

$$\mathbf{K}_0 = \begin{bmatrix} -116.73261635 & -2.48042260 \\ -2.48042260 & -0.77434358 \end{bmatrix}, \quad \mathbf{K}_2 = \begin{bmatrix} 0 & 104.85805076 \\ 0 & 2.29688720 \end{bmatrix},$$

$$\mathbf{H}_{fw} = \begin{bmatrix} 0.91 \\ 0.014408 \end{bmatrix}$$